Talanta 99 (2012) 924–931

Contents lists available at SciVerse ScienceDirect

Talanta

journal homepage: www.elsevier.com/locate/talanta

Electrochemical determination of olmesartan medoxomil using hydrothermally prepared nanoparticles composed SnO_2–Co_3O_4 nanocubes in tablet dosage forms

Mohammed M. Rahman [a,b,*], Sher Bahadar Khan [a,b], M. Faisal [c], Malik Abdul Rub [a,b], Abdulrahman O. Al-Youbi [b], Abdullah M. Asiri [a,b]

[a] Center of Excellence for Advanced Materials Research (CEAMR), King Abdulaziz University, Jeddah 21589, P.O. Box 80203, Saudi Arabia
[b] Chemistry Department, Faculty of Science, King Abdulaziz University, P.O. Box 80203, Jeddah 21589, Saudi Arabia
[c] Advanced Materials and Nano Research Centre and Department of chemistry, Faculty of Sciences and Arts, Najran University, P.O. Box 1988, Najran, 11001, Saudi Arabia

ARTICLE INFO

Article history:
Received 4 March 2012
Received in revised form
23 July 2012
Accepted 25 July 2012
Available online 2 August 2012

Keywords:
SnO_2–Co_3O_4 nanocubes
Hydrothermal method
Optical properties
Olmesartan medoxomil
I–V technique
Sensitivity

ABSTRACT

Low-dimensional nanoparticles composed SnO_2–Co_3O_4 nanocubes (NCs) were prepared by a hydrothermal method using reducing agents. The doped nanomaterials were investigated by UV/vis, powder X-ray diffraction, FT-IR, energy-dispersive X-ray spectroscopy (EDS), and Raman spectroscopy, and field-emission scanning electron microscopy. They were deposited on a silver electrode (AgE, surface area, 0.0216 cm^2) to give a drug sensor with a fast response towards Olmesartan medoxomil (OSM) in 0.1 mol L^{-1} phosphate buffer-phases. The sensor also exhibits higher sensitivity, long-term stability, and enhanced electrochemical response. The calibration plot is linear (r^2=0.9948) over the 0.28 nmol L^{-1}–1.4 μM OSM concentration range. The sensitivity is ~2.083 μA cm^{-2} mmol L^{-1} and the detection limit is 0.17 nmol L^{-1} (at an SNR of 3). We discuss the possible potential uses of this nanoparticles doped semiconductor NCs in terms of drug sensing, which could also be employed for the determination of drugs in quality control of formulation.

1. Introduction

Doped semiconductor nanomaterials have attracted an extensive interest due to their unique properties and potential applications [1,2]. Semiconductors have been recognized as a promising host-material for transition material at room temperature. It is displayed a control morphology and composed of a number of irregular phases with geometrically-coordinated metals and oxide atoms, which stacked alternately along the axes [3,4]. For distinctive physical and chemical properties of nanomaterials, doped materials have been explored the significant attention due to large-surface area and controlled sizes [5–7]. Doped nanomaterials have drawn an enormous interest towards itself due to their extrinsic, remarkable and wonderful qualities in the electrical, optical, thermal, and mechanical properties as compared to their un-doped materials. It is essential for the preparation of nanomaterials in order to achieve the exceptional quality of doped semiconductor structures. Advances in nanotechnology and the conservatory of innovative sensors, nanomaterial, and devices have been regulating a key-task in the fabrication and improvement of very precise, perceptive, accurate, sensitive, and consistent biomolecular sensors. The exploration for even tiny devices accomplished of nano-level imaging and controlling of nanomaterial, the doping materials (even biological, chemical, pathological samples, or drug-sensor) have recently expanded the spotlight of awareness of the scientist, mainly for control monitoring, owing to the amplifying essential for environmental safety and health monitoring [8,9]. Doped semiconductor metal oxides are the model materials for biomolecular drug sensing due to high active surface areas and extensively employed as sensor for the detection, recognition, and quantification of various drug biomolecules [10–12].

Olmesartan medoxomil (5-methyl-2-oxo-1,3-dioxolen-4-yl) methoxy-4-(1-hydroxy-1-methylethyl)-2-propyl-1-{4-[2-(tetrazol-5-yl)-phenyl]phenyl}methylimidazol-5-carboxylate, is a potent and selective angiotensin AT1 receptor blocker-2. Generally, it has been used for the treatment of high-blood pressure (hypertension). The OSM drug contains a medoxomil ester moiety and is cleaved quickly by an endogenous esterase to release the active metabolite olmesartan [13]. Several analytical methods that have been reported for the estimation of OSM in biological fluids and pharmaceutical

* Corresponding author at: Center of Excellence for Advanced Materials Research (CEAMR) and Chemistry Department, Faculty of Science, King Abdulaziz University, P.O. Box 80203, Jeddah 21589, Saudi Arabia.
Tel.: +966 596421830; fax: +966 026952292.
E-mail addresses: mmrahman@kau.edu.sa, mmrahmanh@gmail.com (M.M. Rahman).

0039-9140/$ - see front matter © 2012 Elsevier B.V. All rights reserved.
http://dx.doi.org/10.1016/j.talanta.2012.07.060

formulations include spectrophotometric [14–16], high-performance liquid chromatography (HPLC) [17,18], and highperformance thin-layer chromatography (HP-TLC) [19]. Method for analyses of OSM in biochemical stuffs such as human plasma and urine by florescence and LC–MS/LC–MS–MS has been reported previously [20–23]. The literature survey displayed that several conventional methods are reported for estimation of OSM in biological fluids and in separate or combination with other drugs in dosage form. There is not any electro-analytical method reported for estimation of OSM in bulk and dosage form. The interest of this work is the development of a simple, accurate and sensitive electrochemical method for the determination of OSM in bulk and dosage form. OSM was estimated using LC coupled with fluorescence detection and LC tandem mass-spectrometry, and RP-HPLC [24,25]. HPLC methods for estimation of OSM in tablet dosage forms have also been reported elsewhere [26–30]. To the best of our knowledge, no electrochemical technique has been reported for the sensitive detection of OSM drug using doped nanocomposites in buffer phase till to date. Use of capillary zone electrophoresis for the determination of OSM in pharmaceutical dosage form has also been reported [31–33]. No stability demonstrating assay of OSM in bulk and solid dosage form could be outlined in the literature. The aim of the present study is the development of a simple, reliable, accurate and sensitive electrochemical technique for the detection of OSM on the basis of doped semiconductor metal oxides nanostructure fabricated sensor.

Tin dioxide (SnO_2) is an n-type broad band-gap semiconductor. The potential applications of undoped semiconductor materials have been reported based on sensors and catalysis fields recently [34,35]. The microstructure and electrical response of dense SnO_2-based ceramics have been comprehensively examined since their non-linear electrical action was reported for the first time [36–38]. SnO_2-based powders and devices are obtained by means of a variety of synthesis techniques including the mixed oxides route, wet-chemical process, the polymeric precursor's route, co-precipitation, and sol-gel methods. Although it is a time consuming technique, the use of polymeric precursors have proven significant advantages over the mixed oxides routes. For example, it ensures the uniform distribution of the additives in the final sintered piece [39–41]. In an attitude to innovate SnO_2-based sensors, it has investigated the sensing properties of SnO_2–Co_3O_4 nano-composites. As reported previously, the composite systems of SnO_2 (n-type semiconductor) and Co_3O_4 (p-type semiconductor) showed remarkable sensing characteristics depending on their structural morphologies. Besides, the system containing equal amounts of SnO_2 and Co_3O_4, which showed p-type behavior was fairly sensitive [42]. It was reported that the addition of a small amount of gold to the Co_3O_4 loaded In_2O_3 was effective in improving the sensitivity [43]. Similar promoting effects of gold have been also reported for gold and La_2O_3-doubly loaded SnO_2 sensor [44]. Thus it was executed to additional progress of the sensing behaviors of two types of SnO_2–Co_3O_4 composites in this study.

Doped metal oxide nanomaterial is broadly demonstrated for the detection of drug biomolecules in electrochemical control process due to their several benefits over conventional chemical analysis techniques in term of large-surface area for monitoring in healthcare and drug delivery fields. In conventional method, it was exhibited the slower response, surface fouling, noise, unstable signals, and lower dynamic range as well as lower sensitivity with uncoated nanomaterials electrodes towards OSM detection. Hence, the modification of the sensor surface with codoped nanomaterials is very urgent to attain higher sensitive, repeatable, and stable responses. Therefore, a simple and reliable *I–V* electrochemical approach is urgently required for relatively easy, convenient, and inexpensive instrumentation which displays higher sensitivity and lower detection limits compared to conventional methods. Here, a reliable, large-scale, and highly sensitive *I–V* method is applied for detection of OSM drugs using SnO_2–Co_3O_4 nanocubes. The present approach depicts a simple and reliable sensitive, low-sample volume, ease to handle, and precise electrochemical techniques over the existing UV, LC–MS, and HPLC techniques, which is free from experimental steps or variables. The simple coating method for preparation of nanoparticles thin-film with conducting binders is used for the fabrication of codoped SnO_2–Co_3O_4 NCs films. In present study, low-dimensional nanoparticles composed NCs films with binders are prepared and detected OSM in the phosphate buffer solution (PBS) system by a simple *I–V* method. To best of our knowledge, this is the first report for detection of OSM with codoped SnO_2–Co_3O_4 NCs using easy and reliable *I–V* method in short response time.

2. Experimental sections

2.1. Chemical reagents and apparatus

Tin chloride ($SnCl_4$), cobalt chloride ($CoCl_2$), monosodium phosphate, butyl carbitol acetate, ethyl acetate, disodium phosphate, and all other chemicals used were of analytical grade and obtained from Sigma-Aldrich Company. 0.1 mol L^{-1} PBS at pH 7.0 is prepared by mixing of unimolar concentration of 0.2 mol L^{-1} Na_2HPO_4 and 0.2 mol L^{-1} NaH_2PO_4 solution in 100.0 mL de-ionize water at room conditions. Stock solutions of olmesartan medoxomil ($C_{29}H_{30}N_6O_6$; molecular weight, 558.59) were prepared by dissolving 0.775 mg in 100.0 ml of 0.1 mol L^{-1} PBS and volume was made up to mark in a 100.0 ml calibrated volumetric flask to obtain the saturated stock solution of OSM (0.0138 mmol L^{-1}). The λ_{max} (302.0 nm) of calcined SnO_2–Co_3O_4 NCs was evaluated with UV/visible spectroscopy (Lamda-950, Perkin Elmer, Germany). FT-IR spectra were performed with a spectrophotometer (Spectrum-100 FT-IR) in the mid-IR range, which was purchased from Perkin Elmer, Germany. Raman station 400 (Perkin Elmer, Germany) was used to measure the Raman shift of codoped NCs material using radiation source (Ar^+ laser line, λ; 513.4 nm). The powder X-ray diffraction (XRD) prototypes were assessed with an X-ray diffractometer (XRD; X'Pert Explorer, PANalytical diffractometer) equipped with Cu-K_α1 radiation (λ=1.5406 nm) using a generator voltage of 40.0 kV and a generator current of 35.0 mA applied for the purposed. Morphology of codoped nanomaterial was investigated on FE-SEM instrument (FESEM; JSM-7600F, Japan). *I–V* technique is executed for the investigation of OSM drugs by using Electrometer (Kethley, 6517 A, Electrometer, USA) at room conditions.

2.2. Synthesis and growth mechanism of codoped SnO_2–Co_3O_4 NCs

The solution of starting reactants ($CoCl_2$ and $SnCl_4.2\,H_2O$) is prepared in aqueous medium at room conditions. After addition of NH_4OH (for adjusting the pH) into the mixture of metal chloride solutions, it was stirred gradually for few minutes at room temperature. SnO_2–Co_3O_4 nanocubes have been prepared by adding unimolar concentration of $CoCl_2$ and $SnCl_4$ as starting materials (as reducing agent) into hydrothermal cell (Teflon line autoclave) for 16 h. Initially reactants were gradually dissolved into the de-ionized water to form 0.1 mol L^{-1} concentration individually at room temperature. Then these unimolar solutions were mixed properly and then the solution pH was adjusted (at 11.0) using aqueous NH_4OH; and finally placed into the oven at 150.0 °C for 12 h. The starting materials of $SnCl_4$, $CoCl_2$, and NH_4OH were used without further purification for co-precipitation technique to doped ($Co_3O_4 \cdot SnO_2$) composition. Again NH_4OH

was added drop-wise into the strongly stirred $SnCl_4$ and $CoCl_2$ solutions mixture to produce a significant doped precipitate.

The growth mechanism of doped SnO_2–Co_3O_4 nanocube materials can be elucidated on the basis of chemical reactions and nucleation as well as growth of codoped nanocrystals, which is presented in below

$$NH_4OH_{(aq)} \rightarrow NH_{4\,(aq)}^{+} + OH_{(aq)}^{-} \quad \text{(i)}$$

$$SnCl_4 \cdot 2H_2O + 4NH_4OH_{(aq)} + H_2O_{(aq)} \rightarrow Sn(OH)_{4(aq)} + 4NH_4Cl + 6H_2O_{(aq)} \quad \text{(ii)}$$

$$CoCl_{2(s)} + 2NH_4OH_{(aq)} \rightarrow Co_3O_{4(s)} + 2NH_{4\,(aq)}^{+} + 2Cl_{(aq)}^{-} \quad \text{(iii)}$$

$$Sn(OH)_{4(aq)} + 2NH_4OH_{(aq)} + Co_3O_{4(s)} \rightarrow SnO_{2(s)} \cdot Co_3O_{4(s)} + 2NH_{4\,(aq)}^{+} + 2H_2O \quad \text{(iv)}$$

The reaction is forwarded slowly according to the proposed Eqs. (i)–(iii). During preparation, the pH value of the reaction medium plays an important role in the nanomaterial codoped formation. At a particular pH, when $SnCl_4$ is hydrolyzed with ammonia solution, tin hydroxide is formed instantly according to the Eq. (ii). During the synthesis of nanomaterials, NH_4OH is used to control the pH value (alkaline phase) as well as supplied the hydroxyl ions (OH^-) slowly in reaction medium. When the concentration of Sn^{2+} and OH^- ions is reached to critical value, SnO_2 nuclei formation started. As the high concentration of Co^{2+} ions [reactions (iii)], the nucleation of SnO_2 crystals become slower due to the lower activation energy barrier of heterogeneous nucleation. In presence of Co^{2+} concentration in reaction system, a number of larger $SnO_2 \cdot Co_3O_4$ crystals with nanoparticle aggregated cube-like morphology were formed according to the reactions [Eq. (vi)]. Then the resultant solution was washed thoroughly with acetone and water consecutively and kept for drying at room conditions. Finally, the as-grown doped SnO_2–Co_3O_4 nanocubes materials were calcined at 400.0 °C for 5 h in the muffle furnace (Barnstead Thermolyne, 6000 Furnace, USA). The calcined nanostructures were investigated and characterized in detail in terms of their morphological, structural, optical properties, and applied for OSM drug detection for the first time.

2.3. Fabrication and detection technique of OSM drugs

Silver electrode (AgE) is prepared with calcined SnO_2–Co_3O_4 NCs, where butyl carbitol acetate (BCA) and ethyl acetate (EA) used as a conducting binder. The small amount of mixture (EA, BCA, and NCs) is uniformly mixed and coated on the AgE surfaces and placed it into the oven at 70.0 °C for 12 h until the coating film is completely dry. An electrochemical cell is mounted with doped NCs coated AgE as a working electrode and Pd wire is used a counter electrode. Stock solution of OSM (0.0138 mmol L^{-1}) is diluted at various concentrations and used as a target. Amount of 0.1 mol L^{-1} PBS was kept constant in the beaker as 10.0 mL throughout the chemical investigation. OSM analyte solution is made with various concentrations in the range 0.28 nmol L^{-1}–0.014 mmol L^{-1}. The sensitivity is calculated from the slope of current vs. concentration (I vs. C) from the calibration plot divided by the value of active surface area of fabricated AgE electrodes. Electrometer is used as a voltage sources for the I–V technique in two electrode systems.

3. Results and discussions

3.1. Optical analysis

The optical property of the calcined SnO_2–Co_3O_4 NCs is one of the significant characteristics for the assessment of its photocatalytic activity. The optical absorption spectra of codoped SnO_2–Co_3O_4 NCs are measured by using the UV–vis spectrophotometer in the visible range (200.0–800.0 nm). UV/visible absorption are a technique in which the outer electrons of atoms or molecules

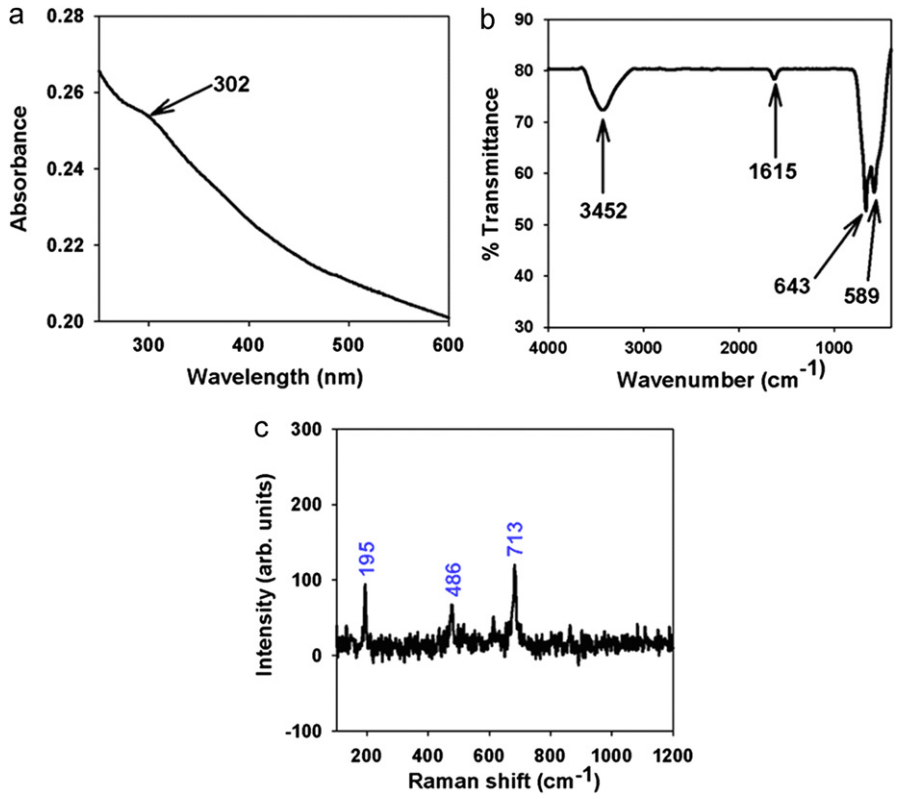

Fig. 1. Typical (a) UV–vis spectrum, (b) FT-IR spectrum, and (c) Raman spectrum of nanoparticles composed SnO_2–Co_3O_4 nanocubes.

absorb radiant energy and undergo transitions to high energy levels. In this phenomenon, the spectrum obtained due to optical absorption can be analyzed to acquire the energy band-gap of the semiconductor. The optical absorption was executed in large range of wavelength with doped nanomaterials at room conditions. From the absorption spectrum, it has been measured the absorbance of the calcined SnO_2–Co_3O_4 NCs is about 302.0 nm, which is presented in Fig. 1a. Band gap energy (E_{bg}) is calculated on the basis of the maximum absorption band of NCs and found to be 4.10596 eV, according to following equation (vii):

$$E_{bg} = \frac{1240}{\lambda}(eV) \quad \text{(v)}$$

Where E_{bg} is the band-gap energy and λ_{max} is the wavelength (302.0 nm) of the NCs. No extra peak associated with impurities and structural defects were observed in the spectrums, which proved that the synthesized nanorods control crystallinity of SnO_2–Co_3O_4 NCs [45].

The SnO_2–Co_3O_4 NCs are also studied in term of the atomic and molecular vibrations. To predict the motivated identification, FT-IR spectra fundamentally in the region of 400–4000 cm^{-1} are investigated at room conditions. Fig. 1b displays the FT-IR spectrum of the SnO_2–Co_3O_4 NCs, which represents band at 589, 643, 1600, and 3452 cm^{-1}. The observed broad vibration bands (at 589 and 643 cm^{-1}) could be assigned as a metal-oxygen (Co–O and Sn–O modes) stretching vibration [46], which is demonstrated the configuration of codoped nanostructure materials. The supplementary vibrational bands may be assigned to O–H bending vibration (1600 cm^{-1}) and O–H stretching (3452 cm^{-1}). The absorption bands at 1600 and 3446 cm^{-1} usually shows from water, which usually semiconductor nanostructure materials absorbed from the environment due to their high surface-to-volume ratio of mesoporous nature [47]. Finally, the experimental vibration bands at low frequencies regions recommended the formation of SnO_2–Co_3O_4 nanocubes.

Raman-spectroscopy is a spectroscopic method employs to reveal vibrational, rotational and other low-frequency phases in Raman active compounds. It is based on inelastic scattering of monochromatic light, generally from a laser in the visible, near infra-red, or near ultra-violet ranges. The laser-light is directly correlated with molecular vibrations, phonons or other excitations in the modes, exhibiting in the energy of the laser photons being moved upwards or downwards. Raman-spectroscopy is generally utilized in material chemistry, since the information is explicit to the chemical bonds and symmetry of metal-oxygen stretching or vibrational modes. Fig. 1c confirms the Raman spectrum (low-region) where key aspects of the wave number are executed at 195, 486, and 713 cm^{-1} for metal-oxygen (Co–O and Sn–O) stretching vibrations. These bands can be assigned to a cubic-phase of nanoparticles composed SnO_2–Co_3O_4 NCs [48].

3.2. Morphological, structural, elemental and chemical analysis:

High resolution FE-SEM images of calcined SnO_2–Co_3O_4 nanocubes are exhibited in Fig. 2a–d (low to high magnification). The images composed of nanoparticles aggregated in cubic-shapes of nanostructures. The average diameter of nanocube is calculated in the range 400–550 nm, which is close to 459.0 nm. The average diameter of nanoparticle is also measured, which is close to 13.0 ± 2.0 nm. It is exhibited clearly from the FE-SEM images that the simple hydrothermal methodology of synthesized doped products are nanostructure of SnO_2–Co_3O_4 NCs, which displayed in an extraordinarily shape, high-density, and obtained nanostructure in almost cube-shapes. It is also suggested that almost all of the nanostructure possessed in spherical nanoparticles composed of cube-shapes of aggregated doped SnO_2–Co_3O_4 nanomaterials.

The electron dispersive spectroscopy (EDS) investigation of calcined SnO_2–Co_3O_4 NCs indicates the presence of Sn, Co, and O composition in the pure calcined codoped material. It is clearly displayed that calcined synthesized materials controlled only tin, cobalt, and oxygen elements, which is presented in Fig. 3(a–c). The composition of Sn, Co, and O is 12.57%, 4.85%, and 82.58% respectively. No other peak related with any impurity has been detected in the EDS, which confirms that the doped products are composed only with Sn, Co, and O.

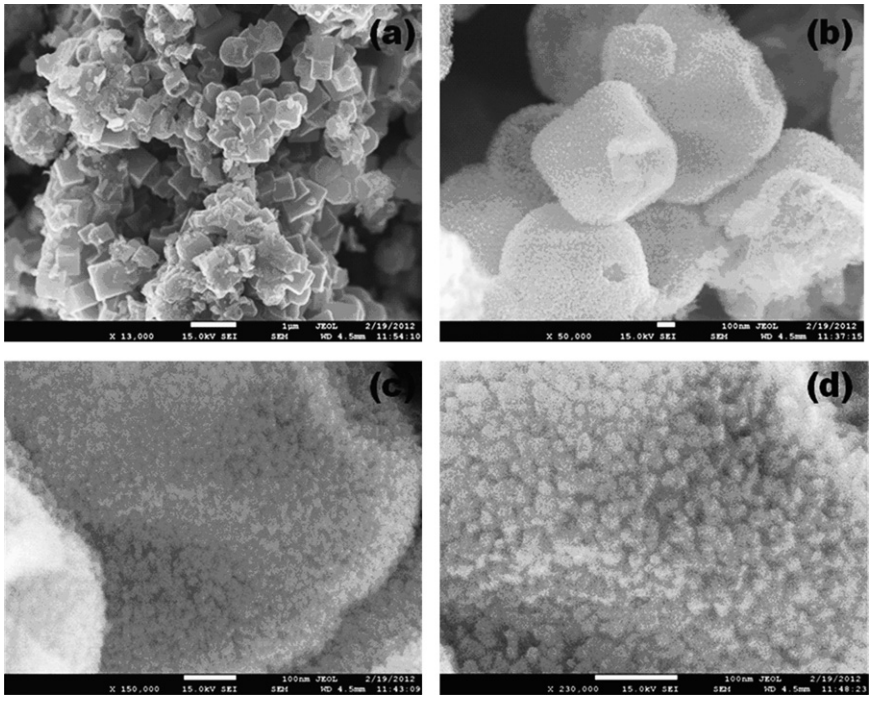

Fig. 2. Low to high-magnified FE-SEM images of codoped SnO_2–Co_3O_4 nanocubes.

Crystallinity and crystal phases of the calcined SnO_2–Co_3O_4 NCs were examined. X-ray diffraction patterns of doped NCs are shown in Fig. 3d. The NC samples were investigated and shown as face centered cubic. The as-grown SnO_2–Co_3O_4 was calcined at 400.0 °C in furnace to start the formation of nano-crystalline codoped phases. Fig. 2d reveals characteristic crystallinity of the combined SnO_2–Co_3O_4 NCs and their aggregative crystal arrangement. The reflection peaks in this prototype were initiated to correspond with Co_3O_4 phase having face-centered-cubic geometry [JCPDS # 01-078-1970]. The phases demonstrated the key feature peaks (with blue color) with indices for calcined crystalline Co_3O_4 at 2θ values of 31.27(220), 36.85(3111), 38.6(222), 44.9(400), 56.45(422), 58.9(511), 72.3(620), and 78.5(622) degrees. The face-centered-cubic lattice parameters are (a, 8.085), point group (Fd-3 m), and radiation ($CuK_\alpha1$, $\lambda=1.5406$). This is confirmed that there is major number and amount of crystalline Co_3O_4 present in codoped NCs. Beside this, all the reflection peaks in this pattern were also observed to match with SnO_2 phase (Cassiterite) having tetragonal geometry [JCPDS # 01-074-9942]. The phases exhibited the major characteristic peaks (black-color) with indices for calcined crystalline SnO_2 at 2θ values of 26.7(111), 34.1(101), 54.5(220), 61.7(310), and 64.9(301) degrees. The tetragonal (unit cell) lattice parameters are $a=4.737$; $c=3.125$; $Z=2$, point group: P42/mnm(136), and radiation: $CuK_\alpha1$ ($\lambda=1.5406$). These indicate that there is considerable amount of crystalline SnO_2 present in codoped nano-structural materials. Finally, the powder X-ray pattern is corresponded to codoped SnO_2–Co_3O_4 NCs, which may be attributed to the doping of Co_3O_4 and SnO_2 lattice site of nanoparticles composed NCs semiconductor nanomaterials [49]. Further, no other impurity peak was observed in the XRD pattern showing the SnO_2–Co_3O_4 phase formation.

X-ray photoelectron spectroscopy (XPS) is a quantitative spectroscopic method that determines the elemental-composition, empirical-formula, chemical-state and electronic-state of the elements that present within a material. XPS spectra are acquired by irradiating a material with a beam of X-rays, while simultaneously determining the kinetic energy and number of electrons that get-away from the top 1–10 nm of the material being analyzed. Here, XPS measurements were executed for SnO_2–Co_3O_4 semiconductor nanomaterials to investigate the chemical states of SnO_2 and Co_3O_4. The XPS spectra of Co2p, Sn3d, and O1s are presented in Fig. 4a. In Fig. 4b, the spin orbit peaks of the $Co2p_{(3/2)}$ and $Co2p_{(1/2)}$ binding energy for all the samples appeared at around 781.9 eV and 793.4 eV respectively, which is in good agreement with the reference data for Co_3O_4 [50]. The O1s spectrum shows a main peak at 527.6 eV with a slight shoulder at ~528.4 eV in Fig. 4c. The peak at 527.6 eV is assigned to lattice oxygen, while the small shoulder at 528.4 eV may be indicated to oxygen (ie, O_2^-) in presence in the doped nanomaterials. XPS was also used to resolve the chemical state of the doped SnO_2 nanomaterial and their depth. Fig. 4d presents the XPS spectra (spin orbit doublet peaks) of the $Sn3d_{(5/2)}$ and $Sn3d_{(3/2)}$ regions recorded with semiconductor doped materials. The binding energy of the $Sn3d_{(5/2)}$ and $Sn3d_{(3/2)}$ peak at 482.7 eV and 491.7 eV respectively denotes the presence of SnO_2 since their bindings energies are similar [51].

3.3. Detection of olmesartan medoxomil drug using doped nanomaterials by I-V technique

With high-mechanical strength, good-conductivity, highly stable, large-surface area, and extremely miniaturized dimension of codoped SnO_2–Co_3O_4 NCs have been widely employed in sensor modification and fabrication of drug detection. The codoped nanomaterials were applied for the detection of OSM in liquid phase system at room conditions. Initially, the thin-film was fabricated using conducting binder and embedded on the AgE electrode. The development technique and fabrication processes are displayed in the graphical diagram (Fig. 5). The PdE and codoped NCs fabricated AgE is used as counter and working electrodes respectively, which is shown in Fig. 5a and b respectively. The OSM was used as a target drug biochemical in buffer phase. The electrical responses in presence of biochemical drugs have been measured using the I–V technique according to the Fig. 5c. The physi-sorption behaviors (adsorption and absorption) as well as detection mechanism of calcined SnO_2–Co_3O_4 NCs are presented in the Fig. 5d. Here the OSM drug bio-molecules are absorbed as well as adsorbed onto the fabricated surfaces in huge amount due it mesoporous natures and large-active surface area of nanostructure material in buffer phase respectively.

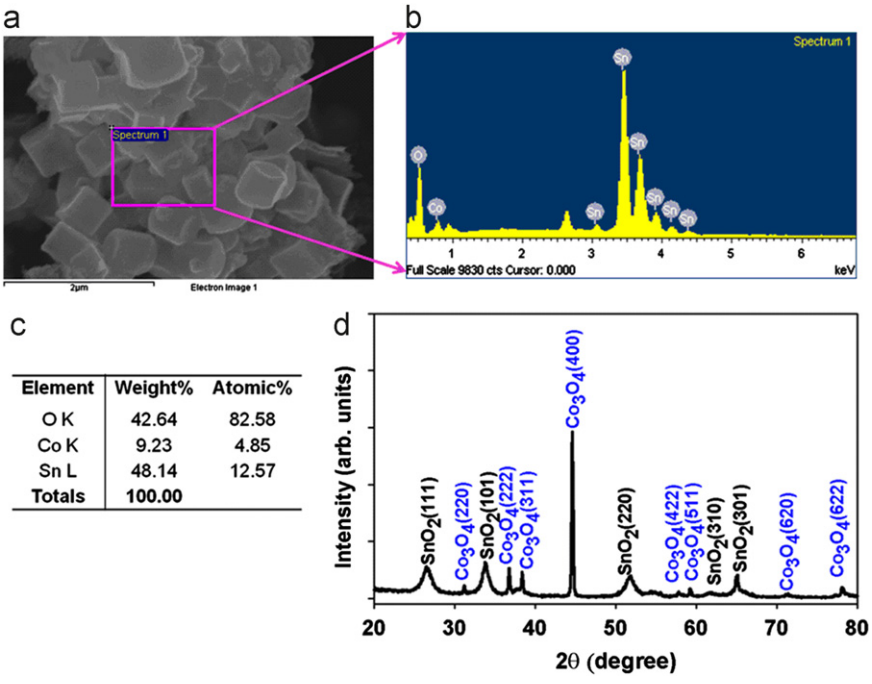

Fig. 3. (a–c) Energy-dispersive X-ray spectroscopy and (d) powder X-ray diffraction of SnO_2–Co_3O_4 nanocubes.

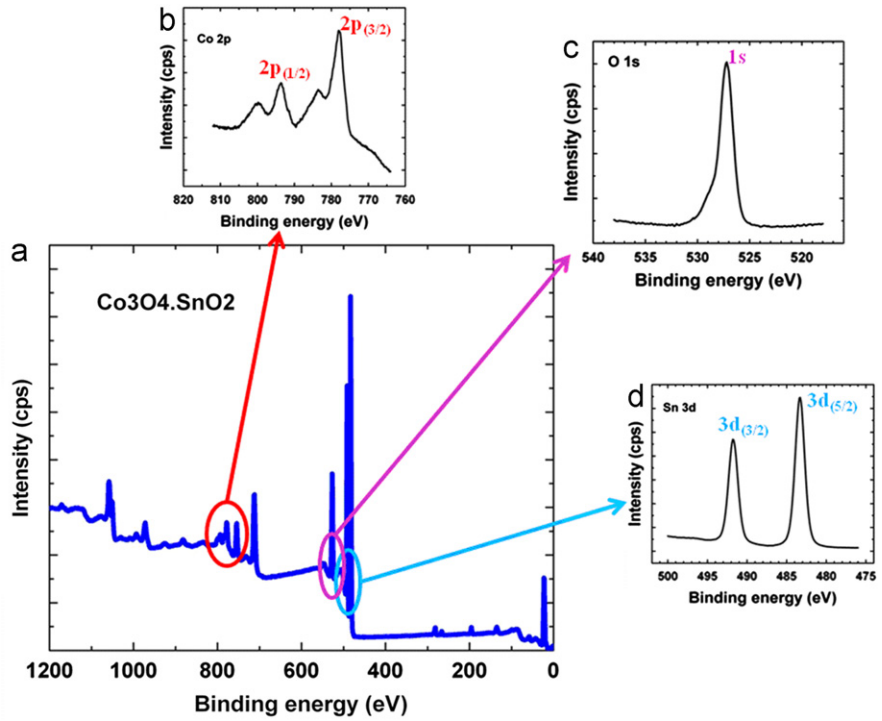

Fig. 4. XPS of (a) doped SnO_2–Co_3O_4 nanomaterials, (b) Co2p level, (c) O1s level, and (d) Sn3d level acquired with MgKα radiation.

Fig. 6a displays the current responses uncoated (gray-dotted) and coated (dark-dotted) AgE working electrode (surface area, 0.0216 cm^2) with doped SnO_2–Co_3O_4 NCs at room conditions. With NCs fabricating surface, the current signal is reduced compared to without fabricated surface, which reveals the surface is slightly blocked with codoped NCs. The current changes for the doped NCs modified electrodes before (dark-dotted) and after (blue-dotted) injection of 50.0 μL OSM (0.28 nmol L^{-1}) in 10.0 mL PBS solution, which is presented in Fig. 6b. These considerable changes of surface current are measured in every injection of the target OSM into the electrochemical solution by Keithley electrometer. 10.0 mL of 0.1 mol L^{-1} PBS solution is originally transferred into the cell and added the low to high concentration of OSM drop-wise from the stock OSM drug solution. *I–V* responses with SnO_2–Co_3O_4 NCs modified electrode surface were evaluated from the different concentrations (0.28–0.014 mmol L^{-1}), which was revealed in Fig. 6c. It shows the current changes of fabricated films as a function of OSM concentration at room conditions. It was also observed that with increasing the concentration of OSM, the resultant currents also increased significantly, which confirmed that the response was a surface process. It shows the response of doped nanomaterials as a function of OSM concentration at room conditions. A large range of OSM concentration was selected to study the probable analytical parameters, which was calculated in 0.28–0.014 mmol L^{-1}. The calibration curve was plotted from the variation of OSM concentrations, which was presented in Fig. 6d. It was exhibited a calibration curve for the response current versus OSM concentration of fabricated SnO_2–Co_3O_4 NCs on AgE sensor. It was measured from the calibration plot that as the concentration of OSM increases, the current response also increases and finally at high OSM concentration, the current reaches at a saturated level which suggests that the active surface sites of NCs saturated with OSM units [52–59]. The sensitivity is executed from the calibration-curve, which is close to 2.0830 μA cm^{-2} mmol L^{-1}. The linear dynamic range of this sensor displays from 0.28 nmol L^{-1}–1.4 μmol L^{-1} (linearity, R=0.9948) and the detection limit was calculated as 0.17 nmol L^{-1} [3 × noise (N)/slope(S)].

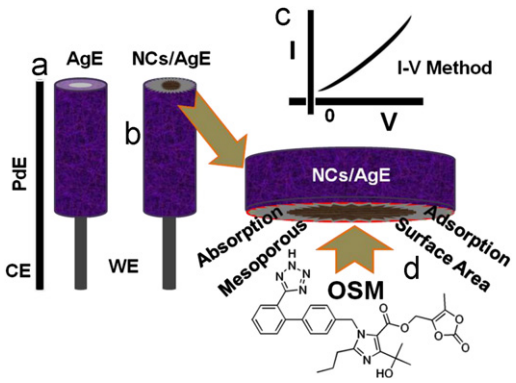

Fig. 5. Fabrication process and methodology of OSM drug detection using calcined nanoparticles composed SnO_2–Co_3O_4 nanocubes. (a) Pd-counter electrode, (b) fabrication of working Ag electrode, (c) expected *I–V* method, and (d) structure and detection mechanism of OSM.

The response time was approximately 10.0 s for the SnO_2–Co_3O_4 NCs coated-electrode to achieve saturated steady state current. The prominent sensitivity of OSM drug sensor can be attributed to good absorption (porous surfaces fabricated with conducting binders) and adsorption ability (large surface area), high catalytic activity, and good biocompatibility of the doped nanoparticles [60–62]. Due to large surface area, NCs are proposed a beneficial nano-environment for the OSM drug detection and recognition with excellent sensitivity. The sensitivity of SnO_2–Co_3O_4 NCs affords high-electron communication features, which enhanced the direct electron communication between the active sites of NCs and sensor electrode surfaces [63,64]. The modified thin NCs coated film had a better reliability as well as stability. However, due to high dynamic surface area, the codoped SnO_2–Co_3O_4 NCs were imposed productive surroundings for the

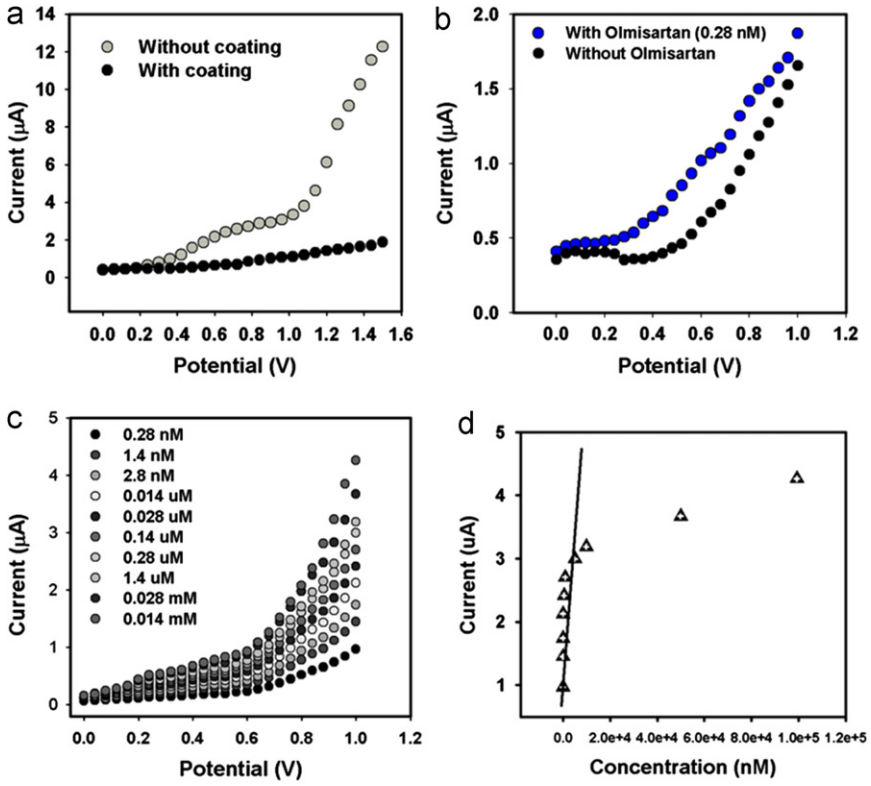

Fig. 6. *I–V* responses of (a) AgE (without modified) and NCs/AgE (with modified); (b) NCs/AgE (without OSM) and NCs/AgE (with OSM); (c) concentration variations (0.28–0.014 mmol L^{-1}) of OSM; and (d) calibration plot of NCs fabricated AgE.

Table 1
Evaluation of the olmesartan medoxomil drug determination using NPs composed SnO_2-Co_3O_4 NCs/AgE electrode performances by *I-V* technique compared with various detection methodologies.

Methods	Range	LDR	Linearity, r^2	No. of repeatation/ samples	LOD	% recovery	Sensitivity	Ref.
Spectroscopic method	–	5–30 μg/mL	0.9998	6	0.14 μg/mL	98.50	–	[11]
RP-HPLC	2–128 μg/mL	–	0.9990	9	0.13 μg/mL	99.65	–	[67]
RP-HPLC	20–100 μg/mL	–	0.9956	–	–	96.70	–	[68]
HP-TLC	–	–	0.9991	6	4.79 ng	99.37	5.328	[69]
RP-HPLC	32–160 μg/mL	–	0.9992	–	–	99.42	–	[70]
RP-HPLC	–	20–100 μg/mL	0.9998	6	–	–	–	[71]
HPLC	–	3.0–20.0 μg/mL	0.9970	6	0.20	99.98	–	[72]
RP-LC & HP-TLC	4–24 μg/mL	–	0.9998	5	0.44 μg/mL	–	–	[73]
UV-spectrophotometry	1–18 mg/mL	–	0.9980	7	0.03 mg/mL	99.30	–	[74]
RP-HPLC-DAD	5–40 μg/mL	–	0.9980	8	–	99.00	0.043	[75]
RP-HPLC	8–24 μg/mL	–	0.9998	3	0.5 μg/mL	–	–	[76]
***I–V* methods**	**0.28 nmol/L–0.014 mmol/L**	**0.28 nmol/L–1.4 μmol/L**	**0.9948**	**10**	**0.17 nmol/L**	**97.30**	**~2.083 μA cm^{-2} mmol/L**	**Current work**

OSM drug biomolecule detection (by adsorption) with enormous quantity [65,66]. To check the repeatability and storage stabilities, *I–V* response for SnO_2–Co_3O_4 NCs coated sensor was examined (up to 2 weeks). After each measurement, the fabricated sensor was washed carefully with the PBS buffer solution and found no significant decreased on the current responses (recovery, 97.3%). The sensitivity was retained almost same of initial sensitivity up to week, after that the response of the fabricated SnO_2–Co_3O_4 NCs sensor gradually decreased. In Table 1, it is compared the performances for olmesartan drug detection based SnO_2–Co_3O_4 NCs using various modified electrode materials.

4. Conclusion

Finally, the codoped nanoparticles aggregated SnO_2–Co_3O_4 NCs are prepared by facile hydrothermal method with controlled structure, which is exposed a constant morphological development in nanostructure materials and potential drug detection applications. Low-dimensional nanoparticles composed NCs are allowed very sensitive transduction of the liquid/surface interactions for OSM detection at room conditions. This opportunity is to emergence a variety of structural morphologies proposed different approaches of modification of the drug biomolecules with

codoped nanostructure materials. Here, NCs are employed to fabricate a simple, efficient, and sensitive OSM detection consisting on side-polished AgE electrode surface. To best of our knowledge, this is the first report for detection of OSM drug with codoped SnO_2–Co_3O_4 NCs using a simple and reliable *I–V* method in short response time. This approach has described for the detection of OSM with doped NCs in various attractive and potential features.

Acknowledgments

Center of Excellence for Advanced Materials Research, King Abdulaziz University, Jeddah, Saudi Arabia is highly acknowledged. Authors are thankful to the Deanship of Scientific Research and Center for Advanced Materials and Nano-Engineering (CAMNE), Najran University, Najran, Saudi Arabia.

References

[1] X. Wang, J. Song, J. Liu, Z.L. Wang, Science 316 (2007) 102.
[2] K. Keren, R.S. Berman, E. Buchstab, U. Sivan, E. Braun, Science 302 (2003) 1380.
[3] D. Chakraborti, J. Narayan, J.T. Prater, Appl. Phys. Lett. 90 (2007) 062504.
[4] L. Shi, C. Pei, Y. Xu, Q. Li., J. Am. Chem. Soc. 133 (2011) 10328.
[5] E.B. Morgado, A. Marinkovic, P.M. Jardim, M.A.S. de-Abreu, F.C.J. Rizzo, Solid State Chem. 182 (2009) 172.
[6] M.M. Rahman, Nanomaterials, INTECH, Open Access Publisher, Inc., Croatia, 2011, pp. 1–356.
[7] D.D. Awschlom, J.F. Smyth, G. Grinstein, D.P. DiVincenzo, D. Loss, Phys. Rev. Lett. 68 (1992) 3092.
[8] Z. Yang, Y. Huang, G. Chen, Z. Guo, S. Cheng, S. Huang, Sensors Actuators. B Chem. 140 (2009) 549.
[9] L. Shi, Y. Xu, S. Hark, Y. Liu, S. Wang, L.M. Peng, K. Wong, Q. Li, Nano Lett. 7 (2007) 3559–3563.
[10] H. Gonga, J.Q. Hu, J.H. Wang, C.H. Ong, F.R. Zhu, Sensors Actuators. B Chem. 115 (2006) 247.
[11] P. Mehulkumar, V. Ramesh, V.V. Kumar, R. Srinivas, P.V. Diwan, Asian J. Res. Chem. 2 (2009) 127.
[12] M.M. Rahman, High-Pressure Electrochemistry and Applications, Lambert Academic Publishers, Inc., Germany, 2011, pp. 1–132.
[13] A.V. Kasture, M. Ramteke, Indian J. Pharm. Sci. 68 (2006) 394.
[14] P.R. Topale, N.J. Gaikwad, M.R. Tajane, Invest. N. Drug 40 (2003) 119.
[15] J.R. Rao, S.S. Kadam, K.R. Mahadik, Invest. N. Drug 39 (2002) 378.
[16] K. Rajeswari, G.G. Sankar, A.L. Rao, J.V.L.N. Seshagirirao, Indian J. Pharm. Sci. 68 (2006) 275.
[17] A.P. Argekar, S.G. Powar, J. Pharm. Biomed. Anal. 21 (2000) 1137.
[18] D. Lui, P. Hu, N. Matsushima, X. Li, L. Li, J. Jiang, J. Chromatogr. B Anal. Technol. Biomed. Life Sci. 856 (2007) 190.
[19] C. Mustafa, A. Sacide, Chromatographia 66 (2007) 929.
[20] P.K. Verma, V.K. Kamboj, S. Ranjan, Int. J. Chem. Tech. Res. 2 (2010) 1129.
[21] K. Kamat, S.C. Chaturvedi, Indian J. Pharm. Sci. 66 (2005) 236.
[22] M. Celebier, S. Altinoz, Pharmazie 62 (2007) 419.
[23] D. Liu, P. Hu, N. Matsushima, J. Chromatogr. B 856 (2007) 190.
[24] L. Bajerski, R.C. Rossi, C.L. Dias, A.M. Bergold, P.E. Froehlich, Chromatographia 68 (2008) 11.
[25] O. Sagirli, A. Önal, S. Toker, D. Şensoy, Chromatographia 66 (2007) 3.
[26] M.M. Rahman, Photo-Fenton's Degradation of Malachite Green Dye, Lambert Academic Publishers, Inc., Germany, 2011, pp. 1–72.
[27] S. Saglik, O. Sagirli, S. Atmaca, L. Ersoy, Anal. Chim. Acta 427 (2001) 253.
[28] E. Satana, S. Altinay, N.G. Goger, S.A. Ozkan, Z. Senturk. J. Pharm. Biomed. Anal. 25.(2001) 1009.
[29] M.M. Rahman, S.B. Khan, A. Jamal, M. Faisal, A.M. Asiri, Microchim. Acta 178 (2012) 99.
[30] M.M. Rahman, A. Umar, K. Sawada, Sensors Actuators B Chem. 137 (2009) 327.
[31] N.J. Shah, B.N. Suhagia, R.R. Shah, N.M. Patel, Indian J. Pharm. Sci. 69 (2007) 834.
[32] M. Batzill, U. Diebold, Prog. Surf. Sci. 79 (2005) 47.
[33] M. Tiemann, Chem. Eur. J. 13 (2007) 8376.
[34] S.A. Pianaro, P.R. Bueno, E. Longo, J.A. Varela, J. Mater. Sci. Lett. 14 (1995) 692.
[35] R. Parra, L.A. Ramajo, M.S. Góes, J.A. Varela, M.S. Castro, Mat. Res. Bull. 43 (2008) 3202.
[36] H. Taib, C.C. Sorrell, Mater. Sci. Forum 561–565 (2007) 973.
[37] A. Mosquera, J.E. Rodríguez-Páez, J.A. Varela, P.R. Buenon, J. Eur. Ceram. Soc. 27 (2007) 3893.
[38] A. Kurz, K. Brakecha, J. Puetz, M.A. Aegerter, Thin Solid Films 502 (2006) 212.
[39] M.P. Pechini, US Patent no. 3330697, 1967.
[40] H. Yamaura, J. Tamaki, K. Moriya, N. Miura, N. Yamazoe, J. Electrochem. Soc. 144 (1997) 158.
[41] U.S. Choi, G. Sakai, K. Shimanoe, N. Yamazoe, Sensors Actuators B Chem. 107 (2005) 397.
[42] K. Fukui, M. Nakane, Sensors Actuators B Chem. 24–25 (1995) 486.
[43] A. Dodd, A. McKinley, T. Tsuzuki, M. Saunders, Mater. Chem. Phys. 114 (2009) 382.
[44] M. Palard, J. Balencie, A. Maguer, J.F. Hochepied, Mater. Chem. Phys. 120 (2010) 79.
[45] X. Chu, H. Zhang, Mod. Appl. Sci. 3 (2009) 177.
[46] F. Rubio-Marcos, V.C. Casilda, M.A. Banares, J.F. Fernandez, J. Catal. 275 (2010) 288.
[47] M. Peiteado, D. Makovec, M. Villegas, A.C. Caballero, J. Solid State Chem. 181 (2008) 2456.
[48] H.K. Jain, R.K. Agrawal, Invest. N. Drug 37 (2000) 196.
[49] V.V. Vaidya, S.M.N. Roy, S.M. Yetal, S.S. Joshi, S.A. Parekh, Chromatographia 67 (2008) 147.
[50] J.G. Kim, D.L. Pugmire, D. Battaglia, M.A. Langell, Appl. Surf. Sci. 165 (2000) 70.
[51] P.A Grutsch, M.V. Zeller, T.P. Fehlner, Inorg. Chem. 12 (1973) 1432.
[52] L. Dongyang, H. Pei, M. Nobuka, L. Xiaoming, L. Li, J. Ji, J. Chromatogr. B 856 (2007) 190.
[53] S.B. Wankhede, A. Prakash, S.S. Chitlange, Asian J. Res. Chem. 1 (2008) 9.
[54] M.M. Rahman, S.B. Khan, A. Jamal, M. Faisal, M.A. Asiri, Sensors Transducers J. 134 (2011) 32.
[55] A. Prakash, K.D. Lone, A. Shukla, R. Mandloi, V. Ghosh, Asian J. Res. Chem. 1 (2008) 80.
[56] T. Murakami, H. Konno-Naoto, F. Onodera, T. Kawasaki, F. Kusu, J Chromatogr. B 47 (2008) 553.
[57] S.J. Rajput, H.A. Raj, Indian J. Pharm. Sci. (2008) 759.
[58] M.M. Rahman, A. Jamal, S.B. Khan, M. Faisal, Superlattices Microstruct. 50 (2011) 369.
[59] M.M. Rahman, S.B. Khan, M. Faisal, A.M. Asiri, K.A. Alamry, Sensors Actuators B: Chem. 171–172 (2012) 932–937.
[60] M.M. Rahman, A. Jamal, S.B. Khan, M. Faisal, J. Nanopart. Res. 13 (2011) 3789.
[61] M.M. Rahman, S.B. Khan, A. Jamal, M. Faisal, A.M. Asiri, Talanta 95 (2012) 18.
[62] M.M. Rahman, S.B. Khan, A. Jamal, M. Faisal, A.M. Asiri, Chem. Eng. J. 193 (2012) 122.
[63] M.M. Rahman, A. Jamal, S.B. Khan, M. Faisal, Biosensors Bioelectron. 28 (2011) 127.
[64] M.M. Rahman, A. Jamal, S.B. Khan, M. Faisal, ACS App. Mater. Interface 3 (2011) 1346.
[65] M.M. Rahman, A. Jamal, S.B. Khan, M. Faisal, J. Phys. Chem. C 115 (2011) 9503.
[66] M.M. Rahman, S.B. Khan, M. Faisal, A.M. Asiri, M.A. Tariq, Electrochem. Acta 75 (2012) 164.
[67] A.R. Chabukswar, B.S. Kuchekar, S.C. Jagdale, D.M. Mehetre, A.S. More, P.D. Lokhande, Arch. Appl. Sci. Res. 2 (2010) 307.
[68] J.A. Kumar, A. Sathya, K.S. Kumar, P. Sagar, B. Prathap, S.B. Lokesh, V. Gopal, Int. J. Res. Pharm. Sci. 1 (2010) 24–27.
[69] D.G.T. Parambi, S.M. Mathew, V Ganesan, A. Jose, K.G. Revikumar, Int. J. Pharm. Sci. Rev. Res. 4 (2010) 36.
[70] K.S. Chouhan, M.V. Bhure, A.T. Hemke, K.R. Gupta, S.G. Wadodkar, Res. J. Pharm. Biol. Chem. Sci. 2 (2010) 78.
[71] N. Jain, R. Jain, J. Banweer, D.K. Jain, Int. J. Curr. Pharm. Res. 2 (2010) 40.
[72] A.S. Birajdar, S.N. Meyyanathan, B. Suresh, Saudi Pharm. J. 17 (2009) 189.
[73] P.D. Bari, A.R. Rote, Chromatographia 69 (2009) 1469.
[74] D.P. Kardile, N.V. Kalyane, T.H. Thakkar, M.R. Patel, R.K. Moradiya, J. Pharm. Sci. Res. 2 (2010) 599.
[75] R.N. Sharma, S.S. Pancholi, Acta Pharm. 60 (2010) 13.
[76] C.V. Patel, A.P. Khandhar, A.D. Captain, K.T. Patel, Eur. J. Anal. Chem. 2 (2007) 159.